A Preliminary Study of Anti-1-Amino-3-^{18}F-Fluorocyclobutyl-1-Carboxylic Acid for the Detection of Prostate Cancer

Shuntaro Oka[1], Ryota Hattori[1], Fumie Kurosaki[1], Masahito Toyama[1], Larry A. Williams[2], Weiping Yu[2], John R. Votaw[2], Yasunori Yoshida[1], Mark M. Goodman[2], and Osamu Ito[1]

[1]Research Center, Nihon Medi-Physics Co., Ltd., Sodegaura, Chiba, Japan; and [2]PET Center and Department of Radiology, Emory University, Atlanta, Georgia

We evaluated the feasibility of anti-1-amino-3-^{18}F-fluorocyclobutyl-1-carboxylic acid (anti-^{18}F-FACBC) in diagnosing prostate cancer (PCa), using a rat orthotopic prostate cancer transplantation (OPCT) model. Furthermore, using in vivo experiments, we examined the potential of anti-^{18}F-FACBC for differentiating between PCa and inflammation and between PCa and benign prostatic hyperplasia (BPH). **Methods:** The OPCT model was developed by transplanting DU145, a human PCa cell line, into the ventral prostate of athymic F344 rats. To develop a dual PCa and inflammation (DPCI) model, MAT-Ly-Lu-B2—a rat PCa cell line—was transplanted subcutaneously into male Copenhagen rats. Streptozotocin was injected into the hind footpad of these rats for inducing popliteal lymphadenitis. For inducing the BPH, normal F344 rats were castrated and injected subcutaneously with testosterone propionate. In biodistribution studies, the rats were injected with anti-^{18}F-FACBC or ^{18}F-FDG and sacrificed at 15 or 60 min after injection. We performed dynamic small-animal PET of the abdominal portion of the OPCT rats for 60 min after the injection of anti-^{18}F-FACBC or ^{18}F-FDG. **Results:** The biodistribution in the OPCT rats at 60 min after injection showed that the uptake of anti-^{18}F-FACBC and ^{18}F-FDG into the PCa tissue was 1.58 $\pm$ 0.40 %ID/cm^3 (percentage injected dose per cm^3) and 1.48 $\pm$ 0.90 %ID/cm^3, respectively ($P > 0.05$). The accumulation of anti-^{18}F-FACBC in the urinary bladder at 60 min after injection was 3.09 $\pm$ 1.43 %ID/cm^3, whereas that of ^{18}F-FDG was 69.31 $\pm$ 16.55 %ID/cm^3 ($P < 0.05$). Consequently, small-animal imaging with anti-^{18}F-FACBC facilitated the visualization of the PCa tissue of the OPCT rats with higher contrast than ^{18}F-FDG. Furthermore, in comparison with ^{18}F-FDG, apparently higher ratios of PCa to inflammation and PCa to BPH accumulation of anti-^{18}F-FACBC were demonstrated in the animal models. **Conclusion:** FACBC PET is believed to be useful not only for the visualization of human PCa but also for differentiating between PCa and inflammation and between PCa and BHP.

Key Words: anti-^{18}F-FACBC; ^{18}F-FDG; prostate cancer; small-animal imaging

J Nucl Med 2007; 48:46–55

Prostate cancer (PCa) is one of the most common tumors, with an increasing incidence in elderly men not only in the United States and the European Union but also in Japan, and it is predicted that the number of patients will be double the existing number in the next decade. The American Cancer Society reports that in 2006, the number of new PCa cases and deaths due to PCa in the United States is expected to be 234,460 and 27,350, respectively (*1*). Approximately 90% of the estimated new cases of PCa are diagnosed at local or regional stages—for example, 5-y relative survival of PCa patients approaches 100% (*1*). Thus, it is very important to determine whether the cancer is located in the prostate lobes only or metastasizes to other organs.

PET with ^{18}F-FDG has proven to be effective for the detection of primaries and metastases in various tumors, including PCa (*2–4*). However, some studies have reported that the imaging of primary PCa with ^{18}F-FDG is hampered by the high radioactivity in urine due to the excretion of ^{18}F-FDG into the urinary bladder (*4,5*). Furthermore, ^{18}F-FDG accumulates in some prostatic diseases with inflammation, such as benign prostatic hyperplasia (BPH) and prostatitis, because ^{18}F-FDG is taken up by inflammatory cells as well as tumor cells (*4*). In addition to ^{18}F-FDG, the feasibility of some PET tracers, such as ^{11}C-choline (*6*) and ^{11}C-acetate (*7*), for the imaging of human PCa has been reported. However, the short life-life of ^{11}C (approximately 20 min) is a drawback in clinical use. Therefore, a new PET tracer is required for the diagnosis of PCa. This tracer should have the following properties: (a) high uptake into the PCa tissue but not in the normal prostate and the BPH, (b) low uptake into inflammatory tissues, and (c) low excretion into the urinary bladder.

Previous studies have shown that 1-aminocyclobutane-^{11}C-carboxylic acid (^{11}C-ACBC), an alicyclic amino acid derivative, can function as a PET tracer in tumor imaging in an animal model (*8*) and humans (*9*). Furthermore, ^{14}C-ACBC showed no affinity for a *Staphylococcus aureus* abscess

Received May 24, 2006; revision accepted Sep. 25, 2006.
For correspondence or reprints contact: Shuntaro Oka, PhD, DVM, Research Center, Nihon Medi-Physics Co., Ltd., Kitasode 3-1, Sodegaura Chiba 299-0266, Japan.
E-mail: shuntaro_oka@nmp.co.jp

and very low total excretion (3.6% in 2 h, after injection) in rats (*10*). On the basis of these results, ACBC appeared to satisfy the previously mentioned 3 properties required for a new PET tracer. Shoup et al. synthesized anti-1-amino-3-^{18}F-fluorocyclobutyl-1-carboxylic acid (anti-^{18}F-FACBC), and this amino acid derivative exhibited slow excretion into the urinary bladder (*11*). We and others (*12*) are performing preliminary studies of this derivative. In the present study, we performed some in vitro and in vivo experiments to evaluate the feasibility of anti-^{18}F-FACBC for the detection of PCa in comparison with ^{18}F-FDG—the commercially available ^{18}F-labeled PET tracer. In addition, the potential of anti-^{18}F-FACBC for differentiating PCa from lymphadenitis and BPH was also evaluated using animal models.

MATERIALS AND METHODS

Synthesis of Tracers

Anti-^{18}F-FACBC used for a small-animal imaging study performed at Emory University was synthesized according to the method described by McConathy et al. (*13*). This method was slightly modified with respect to the deprotection procedure and used for the synthesis of anti-^{18}F-FACBC at Nihon Medi-Physics Co., Ltd. (NMP). The deprotection procedure involved the removal of the Boc group with 1 mL of a mixture of trifluoroacetic acid (TFA) in CH_2Cl_2 (1:2, v/v) for 3 min, the evaporation of TFA by a stream of helium at 80°C, and alkali hydrolysis with 0.3N NaOH (1 mL) for 5 min. The resulting solution that contained anti-^{18}F-FACBC was neutralized with 0.5 mol/L H_3PO_4 (0.4 mL) and passed through an HLB cartridge (Waters). The synthesis was completed within 90 min after the start of synthesis (SOS), with an overall radiochemical yield of 43.5% ± 8.6% SOS (n = 9). Radio–thin-layer chromatography showed 95.3% ± 6.1% (n = 9) radiochemical purity (acetonitrile/methanol/water/acetic acid = 20:5:5:1; R_f = 0.3–0.4).

Synthesis of ^{18}F-FDG was performed according to the method described by Hamacher et al. (*14*) by using an automated synthesis module that is routinely used in our facility.

Cell Culture and In Vitro Uptake Study

All tissue culture materials and reagents were purchased from Invitrogen unless otherwise stated. DU145, an androgen-independent human PCa cell line, and MAT-Ly-Lu-B2 (MLLB2), an androgen-independent rat PCa cell line, were obtained from American Type Culture Collection. DU145 was maintained in Dulbecco's modified Eagle medium (DMEM) supplemented with 4.5 g/L glucose, 100 U/mL penicillin G, 0.1 mg/mL streptomycin, and 10% fetal bovine serum. MLLB2 was maintained in RPMI 1640 medium supplemented with 10 mmol/L *N*-(2-hydroxyethyl)piperazine-*N*′-(2-ethanesulfonic acid), 4.5 g/L glucose, 100 U/mL penicillin G, 0.1 mg/mL streptomycin, and 10% fetal bovine serum. Both cell lines were cultured in a 5% CO_2 incubator at 37°C.

DU145 was harvested at 80%−90% confluence and resuspended in DMEM at 1.6×10^6 cells/mL. The cells were then seeded into a 24-well flat-bottom tissue culture plate (the cell density was 0.8×10^6 cells/well) and subsequently cultured in a 5% CO_2 incubator for 2 d at 37°C. On the day of experiments, the medium was removed from the wells, and the cells were washed 3 times in warm uptake buffer (37°C) with or without D-glucose and natural amino acid concentrations corresponding to the rat plasma level (*15*). After preincubation in 1 mL warmed uptake buffer for 5 min at 37°C, 0.37 MBq anti-^{18}F-FACBC or ^{18}F-FDG dissolved in 10 μL uptake buffer were added to the cell culture and incubated for 5, 15, 30, or 60 min at 37°C in a 5% CO_2 incubator. After the tracer uptake was stopped by the removal of the uptake buffer, the cells were washed twice with ice-cold phosphate buffered saline (PBS) without calcium and magnesium (PBS(–)) and were lysed in 0.5 mL of 0.2N NaOH. The radioactivity in the cells was measured using an automated γ-counter (AccuFLEXγ7001; Aloka).

Preparation of Orthotopic Prostate Cancer Transplantation (OPCT) Model

All procedures of animal handling and experimentation were in accordance with the protocols approved by the Emory University Institutional Animal Care and Use Committee or the Committee on Animal Welfare at NMP. In all animal preparation, animals were anesthetized with diethyl ether, sodium thiopental (1.5–2.0 mg/kg, intraperitoneally), or ketamine/xylazine cocktail (40 and 4 mg/kg, respectively, intramuscularly).

Male F344 nude rats were purchased from CLEA Japan, Inc., and used for tumor transplantation at the age of either 6 or 8–10 wk for biodistribution experiments or for the microPET (Siemens Medical Solutions) imaging study, respectively. DU145 suspended at 2.5×10^7 cells/mL in ice-cold PBS(–) was mixed with the same volume of Matrigel (Beckton Dickinson), and 20 μL of cell suspension (2.5×10^5 cells) were injected into the ventral prostate (VP). The biodistribution experiment or microPET imaging was performed 3–4 wk after the surgery.

Preparation of Dual Prostate Cancer and Inflammation (DPCI) Model

Male Copenhagen (COP) rats were purchased from Charles River Japan, Inc., and used for tumor transplantation. A cell suspension of MLLB2 at 1×10^6 cells/mL was inoculated subcutaneously in the axilla of the 6-wk-old COP rats. The rats were sacrificed 3 wk after tumor transplantation, and a subcutaneous PCa tissue was then excised and minced using a surgical knife. A piece of tumor block (approximately 70–80 mg) was then implanted subcutaneously in the axilla of the 9-wk-old COP rats. Seven days after the implantation, streptozotocin (STZ, 40 mg/(0.08 mL·kg); Sigma-Aldrich) dissolved in citrate buffer (pH 6.0) was injected into the footpad of the left hind legs of the tumor-bearing rats (*16*). The rats were used for experiments on day 3 after inoculation of STZ (= 10 d from the PCa block implantation).

Preparation of BPH Model

Normal male F344 rats were purchased from Charles River Japan, Inc., and were castrated at the age of 6 wk. Starting from 7 d after castration, the rats received a daily injection of testosterone propionate (3 mg/mL in sesame oil, subcutaneously) (Wako Pure Chemical Industries, Ltd.) for 14 d. The rats were used for the experiments on the day after the final injection of testosterone propionate.

Biodistribution

The rats were fasted for at least 4 h before administration of the tracer injection; 7.4 MBq anti-^{18}F-FACBC or ^{18}F-FDG in 0.2 mL saline were injected into the tail vein. Fifteen or 60 min after the injection, the animals were sacrificed by drawing blood from the abdominal aorta. Several tissues were dissected and weighed. During the dissection of OPCT rats, a PCa tissue was separated from the surrounding normal prostate region; the dimensions of

this PCa tissue were measured using a hand-held caliper, and its volume (cm^3) was calculated. The same procedure was followed for calculating the volume of the urinary bladder filled with urine. In the case of DPCI rats, a subcutaneous PCa and popliteal lymph nodes from both hind legs were isolated. In the case of normal rats and BPH rats, the VP was separated from the dorsolateral prostate (DLP). The radioactivity in each tissue was measured using a single-channel γ-counter (Ohyo Koken Kogyo Co., Ltd.), and the tracer uptake was represented as a percentage of the injected dose per organ (%ID) or %ID per gram of tissue (%ID/g). In biodistribution studies using the OPCT rats, the tracer uptake into the PCa tissue and urinary bladder was calculated not only by %ID and %ID/g but also by %ID/cm^3.

Autoradiography

The prostates of the OPCT rats injected with 111 MBq anti-^{18}F-FACBC or ^{18}F-FDG (0.8 mL/head) were excised at 60 min after the tracer injection, frozen in Tissue-Tek OCT compound (Sakura Finetechnical Co., Ltd.), and cooled to −80°C. The frozen samples were cut to obtain 10-μm-thick slices and mounted on glass slides. The imaging plates (Fuji Photo Film Ltd.) were exposed for approximately 3 h with the slices on the glass slides and then processed with a BAS 2500 imaging analyzer (Fuji Photo Film Ltd.). Finally, the slices were stained with hematoxylin–eosin (H–E) by using the standard method.

microPET Imaging

Phantom Imaging Study. A 60-mL plastic tube was filled with water, and a transmission scan was performed with ^{68}Ga for 5 min by using a microPET P4 scanner (Siemens Medical Solutions). Subsequently, a 5-min static scan was performed after the addition of 34 MBq ^{18}F-FDG into the plastic tube (final radioactivity concentration, 566 kBq/mL). The microPET image of the phantom tube was reconstructed by the microPETManager (version 1.5; Siemens Medical Solutions), using the 2-dimensional ordered-subset expectation maximization algorithm. The slice thickness and pixel size were 1.21 mm and 0.95 mm, respectively. The circular region of interest (ROI) was drawn on decay-corrected transverse images of the phantom tube by using ASIPro (version 3.32; Siemens Medical Solutions). The average microPET counts in the ROIs were calculated from 10 central planes that enclosed >90% of the cross-section of the phantom tube; the calibration constant was calculated using the following formula:

$$\text{Calibration constant} = (\text{final radioactivity concentration in phantom tube}) \div (\text{average microPET counts in ROIs}).$$

Animal Imaging Study. The OPCT rats were fasted for at least 4 h before the tracer injection. A 24-gauge catheter, BD Angiocath (0.7 × 19 mm) (Beckton Dickinson), was inserted into the tail vein of rats. The rats were placed near the center of the field of view of the microPET P4 and anesthetized with 1% isoflurane during the imaging.

A transmission scan of the abdominal portion including the prostate was performed using ^{68}Ga for 15 min. Anti-^{18}F-FACBC or ^{18}F-FDG (74 MBq) was injected via the catheter, and dynamic imaging of the abdominal portion was performed 0–60 min after the tracer injection. The frame durations were defined as follows: 30 s × 4 frames, 60 s × 3 frames, 300 s × 5 frames, and 600 s × 3 frames.

All microPET images were reconstructed using the 2-dimensional OSEM algorithm, as described. The square ROIs of the defined size were manually positioned on the PCa tissue, urinary bladder, pancreas (only FACBC microPET images), femoral muscle, and blood vessels, including the abdominal aorta and postcaval vein, on decay-corrected transverse images, and these were placed on the highest area of radioactivity in each tissue. The sizes of the ROIs were as follows: 4 × 4 pixels for the urinary bladder and muscle; 2 × 2 pixels for the PCa tissue, pancreas, and blood vessels. All ROI counts from the dynamic images were converted to kBq/mL by using the calibration constant obtained from the phantom study, and a time–activity curve of each tissue was generated from each ROI. Furthermore, PCa-to-bladder, PCa-to-pancreas, PCa-to-muscle, and PCa-to-blood ratios of anti-^{18}F-FACBC and ^{18}F-FDG uptake were calculated from each ROI.

Radiation Dose Estimates

Six-week-old male Crj:CD(SD)IGS rats were purchased from Charles River Japan, Inc. The rats were fasted for 20 h before the tracer injection. After 15, 30, 60, 120, 180, and 360 min of anti-^{18}F-FACBC (3.08 MBq/(mL·kg)) injection into the tail vein, the animals were sacrificed by drawing blood from the abdominal aorta. Twenty-two different tissues were dissected, and data (%ID/g except for the urinary bladder [%ID]) were obtained as described. The data were fit to a single-component exponential curve using Microsoft EXCEL 2000, and areas under the curves (AUCs) were calculated. The AUCs were corrected for human body weight according to the previous report (*17*) and were expressed as residence times. These residence times were entered into the MIRDOSE3.1 program to calculate the human radiation dose estimate per unit radioactivity.

Statistical Analysis

Data are presented as mean ± SD and were analyzed using the Kruskal–Wallis rank sum test, a nonparametric test. In all cases, $P < 0.05$ was considered significant.

RESULTS

In Vitro Uptake Study

Uptake studies with anti-^{18}F-FACBC and ^{18}F-FDG into DU145 were performed in the absence (buffer A) or presence (buffer B) of natural amino acids and glucose corresponding to the rat plasma level. The uptake of anti-^{18}F-FACBC in buffer A was approximately 3−8 %ID/10^5 cells; a peak was observed at 15 min of incubation (Fig. 1A). In the case of ^{18}F-FDG, the uptake increased with time from approximately 1 %ID/10^5 cells to 9 %ID/10^5 cells. The uptake of anti-^{18}F-FACBC and ^{18}F-FDG in buffer B decreased markedly to <0.2 %ID/10^5 cells and <0.5 %ID/10^5 cells, respectively (Fig. 1B). ^{18}F-FDG uptake increased during incubation, whereas anti-^{18}F-FACBC uptake remained constant for 60 min of incubation.

Biodistribution in OPCT Model

We examined the biodistribution of anti-^{18}F-FACBC and ^{18}F-FDG using the OPCT rats. The rats were sacrificed at 15 or 60 min after injection of the tracer. In the brain, heart, small intestine, testis, mesenteric lymph nodes, and urinary bladder, the accumulation of ^{18}F-FDG was higher than that of anti-^{18}F-FACBC at 15 and 60 min after injection (Table 1). On the other hand, anti-^{18}F-FACBC uptake into the liver, muscle, and pancreas was higher than ^{18}F-FDG

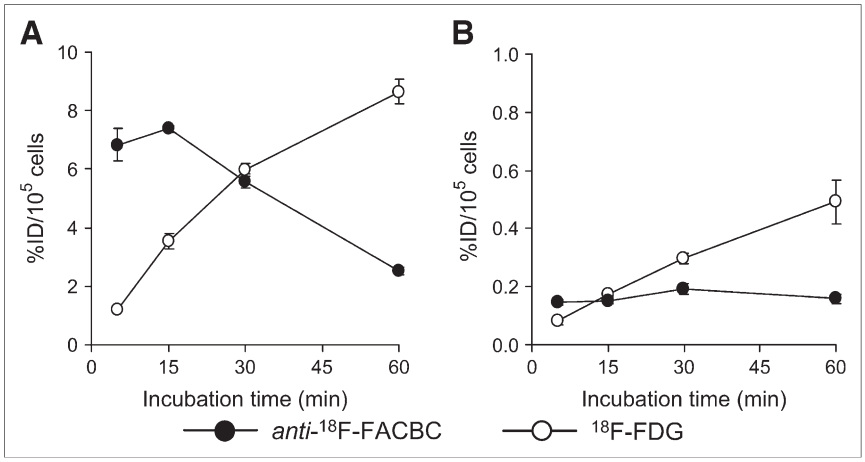

FIGURE 1. Time course of anti-^{18}F-FACBC and ^{18}F-FDG uptake into DU145 in absence (A) or presence (B) of rat plasma concentration of natural amino acids and D-glucose. Each point represents mean ± SD (n = 3).

uptake into these organs at 15 and 60 min after injection. The uptake of anti-^{18}F-FACBC and ^{18}F-FDG into the PCa tissue was almost the same at 15 and 60 min after injection. In contrast, ^{18}F-FDG uptake into the normal prostate regions tended to be slightly higher than anti-^{18}F-FACBC. These results were supported by autoradiography studies using the prostate of the OPCT rats. The PCa tissue was imaged with high contrast in the anti-^{18}F-FACBC autoradiograph (Fig. 2A). The VP showed a marked ^{18}F-FDG accumulation when compared with the PCa tissue and DLP (Fig. 2C). Since a higher accumulation of ^{18}F-FDG in the VP was also observed in normal rats without tumor transplantation (data not shown), this probably resulted from the physiologic accumulation of ^{18}F-FDG in the VP of rats.

A notable difference in the biodistribution of anti-^{18}F-FACBC and ^{18}F-FDG was observed on excretion into the urinary bladder (Table 1). The accumulation of anti-^{18}F-FACBC in the urinary bladder at 60 min after

TABLE 1
Biodistribution of Anti-^{18}F-FACBC and ^{18}F-FDG in OPCT Rats (n = 3)

Tissue* (%ID/g)	Anti-^{18}F-FACBC		^{18}F-FDG	
	15 min	60 min	15 min	60 min
Blood	0.38 ± 0.02†	0.30 ± 0.01	0.71 ± 0.09	0.23 ± 0.09
Brain	0.14 ± 0.02†	0.27 ± 0.01†	1.64 ± 0.20	2.26 ± 0.13
Heart	0.58 ± 0.12†	0.46 ± 0.02†	1.80 ± 0.51	2.04 ± 0.78
Lung	0.78 ± 0.11	0.58 ± 0.03	0.72 ± 0.25	0.64 ± 0.09
Liver	1.84 ± 0.32†	1.12 ± 0.09†	0.70 ± 0.09	0.26 ± 0.04
Spleen	0.87 ± 0.08†	0.63 ± 0.04†	0.73 ± 0.05	0.86 ± 0.07
Kidneys	0.87 ± 0.09†	0.62 ± 0.02	1.35 ± 0.16	0.56 ± 0.05
Small intestine	0.82 ± 0.16†	0.58 ± 0.07†	1.10 ± 0.06	1.22 ± 0.10
Large intestine	0.33 ± 0.05†	0.28 ± 0.01	0.22 ± 0.02	0.26 ± 0.02
Testis	0.19 ± 0.02†	0.26 ± 0.02†	0.48 ± 0.02	0.84 ± 0.07
Bone	0.50 ± 0.03	0.41 ± 0.05†	0.49 ± 0.04	0.57 ± 0.02
Muscle	0.24 ± 0.02†	0.34 ± 0.02†	0.18 ± 0.01	0.16 ± 0.02
Pancreas	2.63 ± 0.15†	2.42 ± 0.16†	0.40 ± 0.07	0.34 ± 0.05
Mesenteric lymph node	0.41 ± 0.12†	0.27 ± 0.03†	0.72 ± 0.12	0.69 ± 0.05
Prostate, normal regions	0.46 ± 0.04†	0.37 ± 0.06	0.90 ± 0.42	0.55 ± 0.18
PCa	1.23 ± 0.22	1.12 ± 0.19	0.94 ± 0.18	1.08 ± 0.38
%ID				
Urinary bladder	0.42 ± 0.14†	0.77 ± 0.12†	13.39 ± 0.48	29.86 ± 1.26
%ID/cm^3				
Urinary bladder	1.93 ± 0.97†	3.09 ± 1.43†	71.22 ± 30.27	69.31 ± 16.55
PCa	1.23 ± 0.49	1.58 ± 0.40	1.08 ± 0.53	1.48 ± 0.90

*Tracer uptake into each tissue is represented as %ID/g, except for urinary bladder. For PCa tissue, tracer uptake is represented as %ID/g and %ID/cm^3. Excretion of tracers into urinary bladder is represented as %ID and %ID/cm^3.

†$P < 0.05$, anti-^{18}F-FACBC vs. ^{18}F-FDG at 15 and 60 min after injection.

Data are presented as mean ± SD.

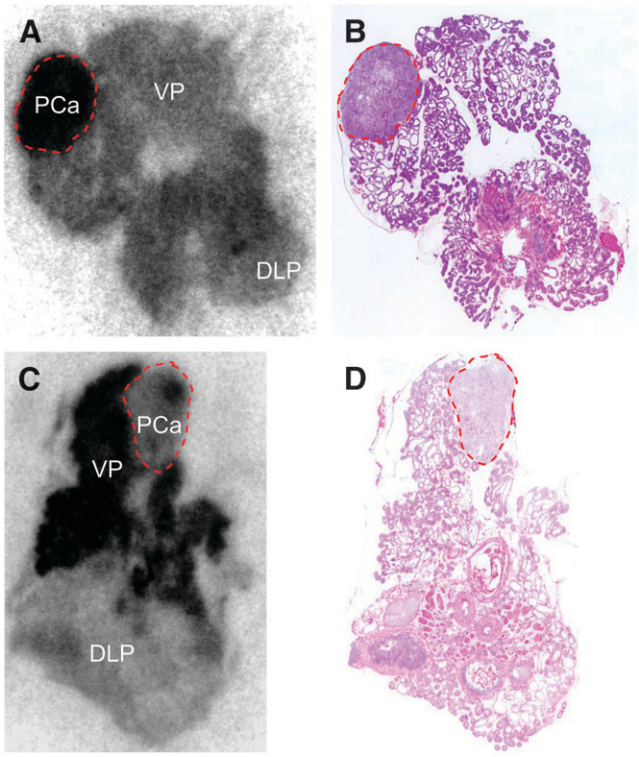

FIGURE 2. Anti-^{18}F-FACBC (A) and ^{18}F-FDG (C) autoradiographs and corresponding sections (B and D, respectively; H–E staining) of prostate from OPCT rats. PCa region is represented with a red dash line.

injection was <1 %ID, whereas that of ^{18}F-FDG was approximately 30 %ID. The ratios of PCa-to-urinary bladder accumulation of anti-^{18}F-FACBC and ^{18}F-FDG at 15 min after injection were 0.78 ± 0.59 (range, 0.35–1.45) and 0.02 ± 0.01 (range, 0.01–0.03), respectively ($P < 0.05$) (Table 2), and those at 60 min after injection were 0.54 ± 0.12 (range, 0.41–0.64) and 0.02 ± 0.01 (range, 0.01–0.03), respectively ($P < 0.05$). Furthermore, the accumulation ratios of tumor to lymph node and tumor to brain were higher in anti-^{18}F-FACBC at 15 min and 60 min after injection (Table 2).

microPET Imaging in OPCT Model

Phantom Imaging Study. From the phantom imaging study, the average microPET counts in the ROIs were calculated as 0.00651. Accordingly, the calibration constant was calculated as 86.9 MBq/mL (= 1 microPET count) by using the formula given earlier.

Animal Imaging Study. Figure 3 shows dynamic transverse images of the FACBC microPET scan (Fig. 3A) and FDG microPET scan (Fig. 3B), and the autopsy specimens of the prostate from the OPCT model (Figs. 3C and 3D). FACBC and FDG microPET imaging studies were performed using 3 and 2 OPCT rats, respectively. As shown in Figure 3A, the PCa (size, 6 × 5 × 5 mm; weight, 106 mg; Fig. 3C) was clearly visualized with anti-^{18}F-FACBC from 20 to 30 min after injection. Similar results were obtained for the other 2 rats (PCa size, 8 × 5 × 4 mm and 8 × 5 × 4 mm; weight, 83.5 and 98.6 mg) in FACBC microPET imaging studies (data not shown). On the other hand, in the FDG microPET images (Fig. 3B), one PCa tissue (size, 6 × 6 × 5 mm; weight, 66.4 mg; Fig. 3D) was visualized, although it was not clear. Another PCa tissue (size, 8 × 6 × 3 mm; weight, 76.8 mg), however, could not be visualized (data not shown).

Figure 4 shows the time–activity curves and the PCa-to-tissue ratios of tracer accumulation. Although anti-^{18}F-FACBC accumulation in the PCa tissue was slightly higher than ^{18}F-FDG accumulation throughout the dynamic scans for 60 min, the accumulation of anti-^{18}F-FACBC in the urinary bladder was extremely low compared with that of ^{18}F-FDG (Fig. 4A). The PCa-to-bladder accumulation ratio of anti-^{18}F-FACBC was approximately 5–7 during the microPET imaging, whereas the PCa-to-blood and PCa-to-muscle ratios were approximately 1 and 2, respectively (Fig. 4B). In contrast, although the PCa-to-muscle accumulation ratio of ^{18}F-FDG was excellent during the dynamic

TABLE 2
PCa-to-Tissue Accumulation Ratios of Anti-^{18}F-FACBC and ^{18}F-FDG in DPCI Rats (n = 3)

Tissue*	Anti-^{18}F-FACBC		^{18}F-FDG	
	15 min	60 min	15 min	60 min
Urinary bladder†	0.78 ± 0.59‡	0.54 ± 0.12‡	0.02 ± 0.01	0.02 ± 0.01
Blood	3.30 ± 0.56‡	3.71 ± 0.78	1.33 ± 0.10	4.73 ± 0.34
Muscle	5.14 ± 0.99	3.25 ± 0.39‡	5.13 ± 0.56	7.18 ± 3.91
Bone	2.49 ± 0.49	2.80 ± 0.76	1.95 ± 0.41	1.87 ± 0.62
Lymph node	3.32 ± 1.39‡	4.13 ± 0.83‡	1.34 ± 0.30	1.56 ± 0.51
Lung	1.69 ± 0.16‡	1.93 ± 0.28	1.36 ± 0.20	1.69 ± 0.53
Liver	0.83 ± 0.26‡	1.01 ± 0.16‡	1.35 ± 0.12	4.98 ± 1.15
Brain	8.56 ± 0.39‡	4.16 ± 0.83‡	0.59 ± 0.19	0.47 ± 0.15

*All ratios were calculated from values of %ID/g, except for ratio of PCa to urinary bladder.
†Ratios were calculated from values of %ID/cm^3.
‡$P < 0.05$, anti-^{18}F-FACBC vs. ^{18}F-FDG at 15 and 60 min after injection.
Data are presented as mean ± SD.

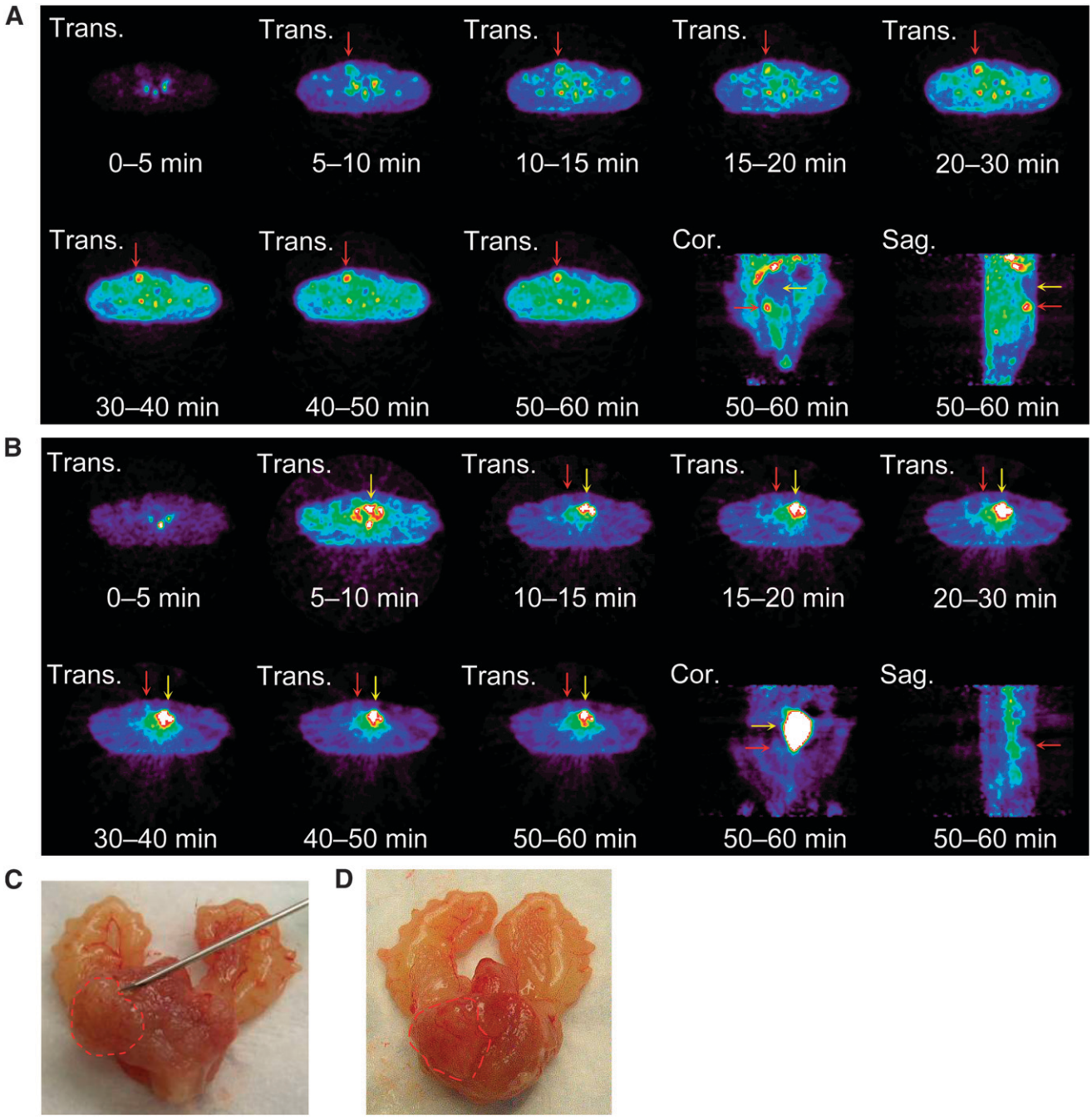

FIGURE 3. (A and B) Dynamic transverse (Trans.) images of PCa region from FACBC microPET scan (A) and FDG microPET scan (B) of OPCT model and coronal (Cor.)/sagittal (Sag.) images corresponding to transverse section. Red and yellow arrows represent the PCa and urinary bladder, respectively. (C and D) Autopsy specimens of prostate of OPCT rats used for FACBC microPET (C) and FDG microPET (D) imaging studies. PCa region is represented with a red dashed line.

scan, the PCa-to-bladder accumulation ratio after 15 min of tracer injection was approximately 0.01 (Fig. 4B).

DPCI Model

To examine the property of anti-^{18}F-FACBC for differentiating tumor from inflammation, we established a rat DPCI model. Biodistribution studies using the DPCI model showed that, although the uptake of anti-^{18}F-FACBC and ^{18}F-FDG into the popliteal lymphadenitis (0.69 ± 0.15 %ID/g and 1.65 ± 0.38 %ID/g, respectively) was higher than those into the intact popliteal lymph nodes (0.31 ± 0.03 %ID/g and 0.46 ± 0.10 %ID/g, respectively) ($P < 0.01$ for both tracers), the uptake ratios of lymphadenitis to intact lymph node were higher for ^{18}F-FDG when compared with that for anti-^{18}F-FACBC (Fig. 5). On the other hand, because the accumulation of anti-^{18}F-FACBC

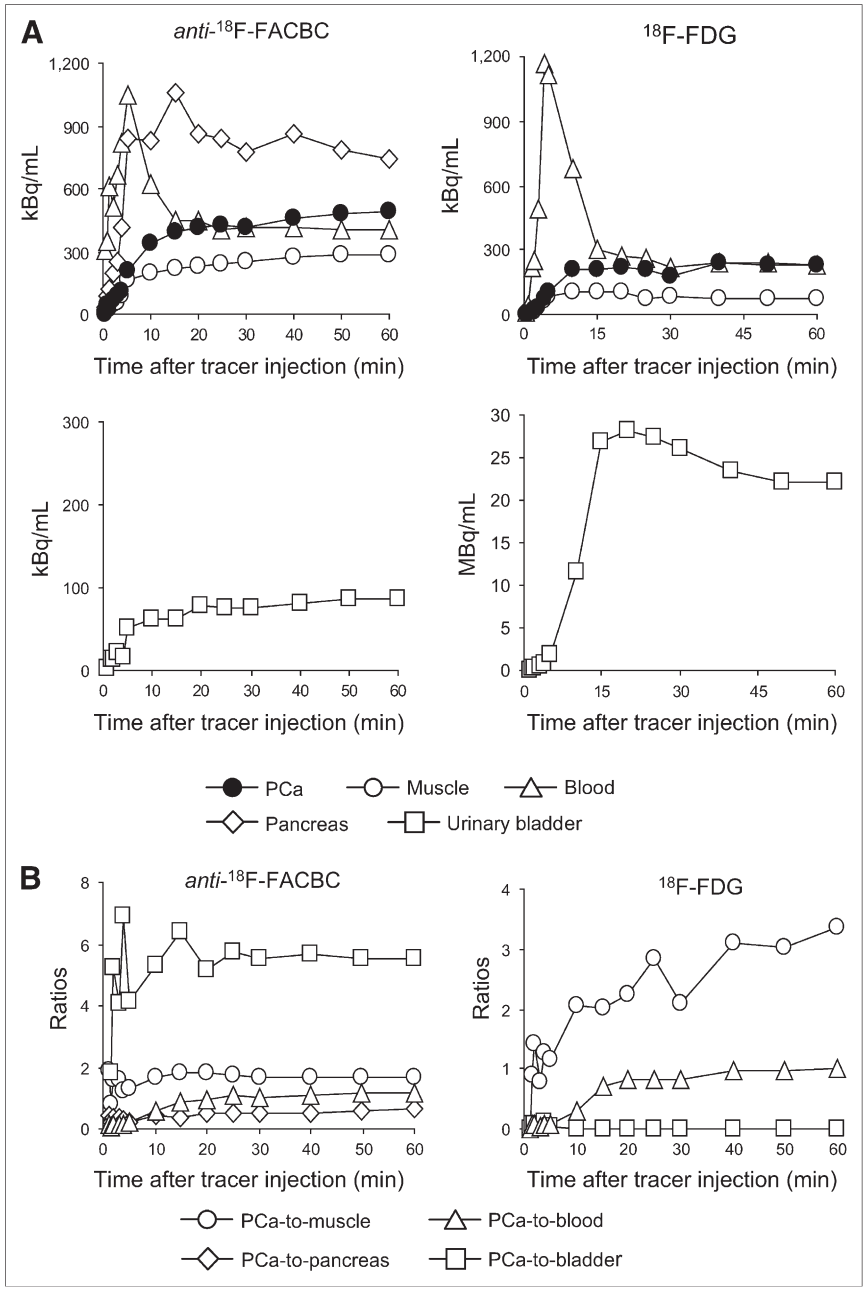

FIGURE 4. (A) Time–activity curves of anti-^{18}F-FACBC (n = 3) and ^{18}F-FDG (n = 1) for PCa, muscle, pancreas, blood, and urinary bladder from OPCT rats. (B) Time course of anti-^{18}F-FACBC (n = 3) and ^{18}F-FDG (n = 1) uptake ratios of PCa to muscle, PCa to blood, PCa to pancreas, and PCa to bladder.

and ^{18}F-FDG in the subcutaneous PCa was almost the same (1.89 ± 0.04 %ID/g and 2.18 ± 0.10 %ID/g, respectively), the accumulation ratio of PCa to lymphadenitis was higher in anti-^{18}F-FACBC than that in ^{18}F-FDG (2.88 ± 1.03 vs. 1.36 ± 0.34; $P < 0.05$).

BPH Model

To compare the property of anti-^{18}F-FACBC with ^{18}F-FDG in the differential diagnosis of PCa and BPH, we established a rat BPH model induced by daily injection of testosterone propionate. We observed an increase in the weight of the prostate from rats injected with testosterone propionate—that is, the VP from the normal and BPH rats weighed 0.12 ± 0.01 g and 0.21 ± 0.03 g, respectively ($P < 0.01$), and the ratio was 1.75. Similarly, the DLP weighed 0.25 ± 0.05 g and 0.33 ± 0.06 g, respectively ($P < 0.05$), and the ratio was 1.3.

The accumulation of ^{18}F-FDG in the VP of the normal ($P < 0.05$) and BPH ($P < 0.01$) rats was clearly higher than that of anti-^{18}F-FACBC (Fig. 6). ^{18}F-FDG accumulation in the VP of the BPH models was higher than that of normal rats ($P < 0.05$); however, no difference was observed in ^{18}F-FDG accumulation between the VP of the BPH rats and the PCa of the DPCI rats. The accumulation of anti-^{18}F-FACBC in the VP of the normal and BPH rats was 0.46 ± 0.07 %ID/g and 0.58 ± 0.04 %ID/g,

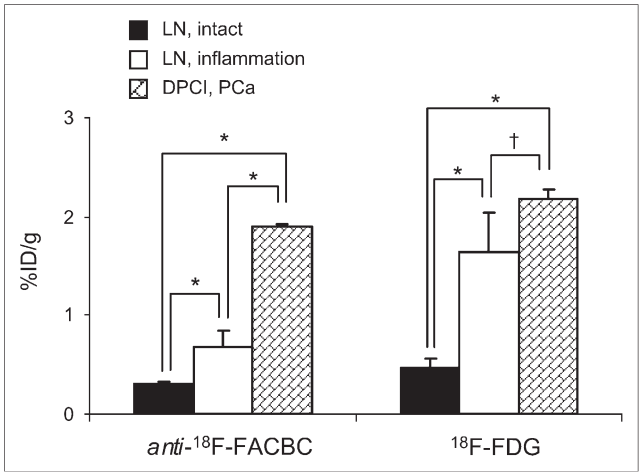

FIGURE 5. Comparison of uptake of anti-^{18}F-FACBC and ^{18}F-FDG at 60 min after injection into normal popliteal lymph node (LN, intact), popliteal lymphadenitis (LN, inflammation, 3 d after STZ stimulation), and subcutaneous PCa in DPCI model. $^{*}P <$ 0.01; $^{\dagger}P$ = not significant. Each bar represents mean ± SD (n = 4).

respectively ($P < 0.05$), indicating that these values were obviously lower ($P < 0.05$) than that of anti-^{18}F-FACBC accumulation in the PCa tissue of the DPCI rats (1.89 ± 0.04 %ID/g).

Radiation Dose Estimates for Anti-^{18}F-FACBC

Human radiation dosimetry estimates for anti-^{18}F-FACBC were calculated as described in the text. The highest and lowest absorbed doses (mGy/MBq) were calculated to be 0.050 to pancreas and 0.007 to brain, respectively. The absorbed doses from anti-^{18}F-FACBC to liver, kidney, small intestine, urinary bladder wall, red marrow, bone surface, and testis were calculated to be 0.038, 0.027, 0.022, 0.018, 0.010, 0.009, and 0.009, respectively. The effective dose equivalent was 0.018 mSv/MBq.

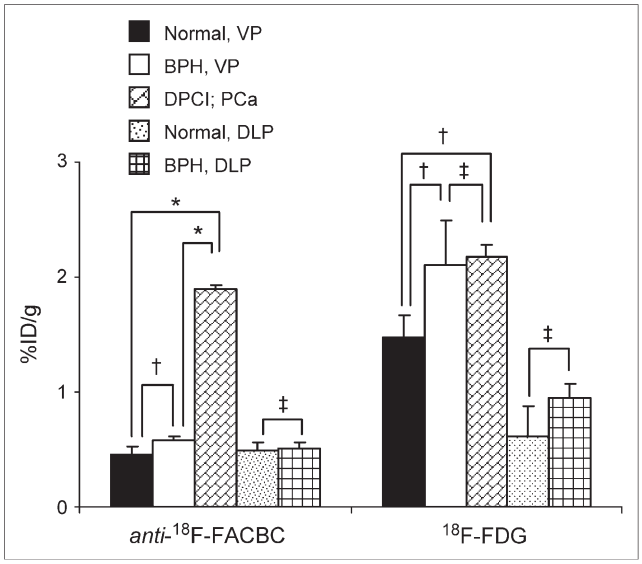

FIGURE 6. Comparison of anti-^{18}F-FACBC and ^{18}F-FDG uptake (%ID/g) into prostate lobes of normal, BPH, and DPCI rats. $^{*}P <$ 0.01; $^{\dagger}P <$ 0.05; $^{\ddagger}P$ = not significant. Each bar represents mean ± SD (n = 3–6).

DISCUSSION

In the present study, we compared the uptake of anti-^{18}F-FACBC into DU145 with that of ^{18}F-FDG in in vitro experiments. In the uptake buffer without natural amino acids and glucose, the highest uptake values of anti-^{18}F-FACBC and ^{18}F-FDG into DU145 were almost the same. However, the highest uptake of anti-^{18}F-FACBC and ^{18}F-FDG was observed at 15 and 60 min of incubation, respectively. This result suggests that anti-^{18}F-FACBC has a higher affinity for DU145 than ^{18}F-FDG in the absence of natural amino acids and glucose.

Although the reason(s) for the decrease in the uptake of anti-^{18}F-FACBC from 15 min of incubation remains to be elucidated, it is possible that anti-^{18}F-FACBC is effluxed from the intracellular space to extracellular space. The transport of anti-^{18}F-FACBC into tumor cells would be mediated at least by system L amino acid transporters (AATs). This is because the uptake of anti-^{18}F-FMeACBC, which possesses a fluoromethyl group at the C-3 position of ACBC and shows a result similar to the biodistribution of anti-^{18}F-FACBC in the tumor-bearing rats, into 9 L gliosarcoma cells was strongly inhibited by a specific inhibitor of system L—namely, 2-aminobicyclo[2,2,1]heptane-2-carboxylic acid (BCH) (*18*). Among the system L AATs, LAT1-4F2hc and LAT2-4F2hc function as amino acid exchangers (*19*). Furthermore, anti-^{18}F-FACBC may not be metabolized and remains intact in cells, similar to ^{14}C-ACBC (*8*). Therefore, it could be considered that anti-^{18}F-FACBC transported into the cells was effluxed from the cells via system L AATs between 15 and 60 min of incubation in the uptake buffer without natural amino acids, as shown in Figure 1. On the other hand, the uptake of anti-^{18}F-FACBC was constant during the incubation period in the uptake buffer modified with natural amino acids and glucose concentrations corresponding to the rat plasma level; this indicates that the influx and efflux of anti-^{18}F-FACBC are balanced under physiologic conditions. In fact, the accumulation of anti-^{18}F-FACBC in the PCa tissue continued throughout the microPET imaging (Figs. 3 and 4). We are currently investigating the mechanism of uptake and intracellular fate of anti-^{18}F-FACBC.

To qualify as an imaging agent for PCa, anti-^{18}F-FACBC should not only show a high accumulation in PCa but also provide high contrast between the PCa tissue and urinary bladder. Using the OPCT rat model, we demonstrated that the slow excretion into the urinary bladder and the high PCa-to-bladder accumulation ratio of anti-^{18}F-FACBC is in sharp contrast to ^{18}F-FDG (Figs. 3 and 4). As shown in Figures 3C and 3D, the PCa tissues involve more than half of the right VP of the OPCT rats; this model is therefore defined as T2b by the TNM staging system (N0 M0).

Accordingly, if the results of the microPET imaging study are applicable to humans, the PCa of stage T2b may be visualized with anti-^{18}F-FACBC but not ^{18}F-FDG. In fact, the low accumulation of ^{18}F-FDG in some PCa of T2 stage was reported (*5*). On the other hand, the properties of anti-^{18}F-FACBC, which shows the slow excretion into the urinary bladder and the high PCa-to-bladder accumulation ratio, were confirmed by Schuster et al., in a preliminary study of PCa patients, although the T stage was not defined in this study (*20*). These results indicate the feasibility of anti-^{18}F-FACBC for the detection of PCa in clinical use.

The mechanism underlying the slow excretion of anti-^{18}F-FACBC remains to be elucidated. It has been reported that some AATs, including B^0AT, are expressed in the epithelial cells of the apical membrane to reabsorb amino acids from the proximal tube of the kidneys (*21,22*). On the other hand, AATs, including TAT1, y^+LAT1-4F2hc, LAT2-4F2hc, and LAT4, are expressed in the cells forming the basolateral membrane of the proximal or distal tubule and the collecting duct in the kidney to efflux or to influx amino acids (*22–24*). If these AATs mediate the uptake of anti-^{18}F-FACBC, it would be reabsorbed from the kidneys. Hence, the excretion of anti-^{18}F-FACBC into the urinary bladder is considered to be slow.

It is well known that PCa metastasizes mainly to the bone and lymph nodes. In biodistribution studies using the OPCT model, the uptake ratio of PCa to lymph node of anti-^{18}F-FACBC was obviously higher than that of ^{18}F-FDG, although there was no significant difference in the PCa-to-bone ratio between both tracers (Table 2). It is reported that sentinel lymph nodes of human PCa are mainly located along the hypogastric artery, followed by in the obturator fossa and the external iliac area (*25*). Consequently, it is expected that anti-^{18}F-FACBC, which exhibits low intrapelvic radioactivity, would be useful for the detection of the metastatic foci of PCa in the sentinel lymph nodes. Furthermore, our study using the DPCI model indicated that the PCa-to-inflammation accumulation ratio of anti-^{18}F-FACBC was higher than that of ^{18}F-FDG (Fig. 5); this suggests the possibility of the differentiation between the metastatic lymph nodes and lymphadenitis by using anti-^{18}F-FACBC.

Some studies have reported that the differential diagnosis between PCa and BPH is difficult using ^{18}F-FDG (*4*). This is because most BPH contains prostatitis in the prostatic lobes. Thus, a relatively high amount of ^{18}F-FDG accumulates in BPH (*4*). As a result, ^{18}F-FDG cannot differentiate between BPH and PCa. In the BPH model, the accumulation of anti-^{18}F-FACBC in rat BPH was at the same level as that in the normal prostate; however, it was clearly low when compared with that in the PCa tissue from the DPCI rats (Fig. 6). This indicates the potential of anti-^{18}F-FACBC for differentiating between BPH and PCa. However, the present study is a preliminary study, and further experiments are required to demonstrate the potential of anti-^{18}F-FACBC for the differential diagnosis.

CONCLUSION

This study demonstrated a marked uptake of anti-^{18}F-FACBC into the PCa tissue in the in vitro and in vivo experiments. In comparison with ^{18}F-FDG, microPET imaging with anti-^{18}F-FACBC facilitated the visualization of the PCa tissue of the OPCT rats with higher contrast. This suggests the feasibility of anti-^{18}F-FACBC as a PET tracer for the diagnosis of human PCa. Furthermore, the PCa-to-inflammation and PCa-to-BPH ratios of anti-^{18}F-FACBC accumulation were higher than those for ^{18}F-FDG. Hence, anti-^{18}F-FACBC may be useful for differentiating between tumor and inflammation and between PCa and BPH. However, the present study is preliminary, and the following issues are not yet elucidated: the mechanism of anti-^{18}F-FACBC uptake into the PCa tissue and inflammatory cells; the mechanism of anti-^{18}F-FACBC excretion into the urinary bladder; and the relationship between anti-^{18}F-FACBC uptake level and 4 parameters—tumor size, tumor malignancy (tumor grade), PSA contents, or type of PCa (e.g., androgen sensitivity). Hence, additional studies using ^{18}F- or ^{14}C-labeled anti-FACBC are in progress at our research center.

ACKNOWLEDGMENTS

The authors thank Masaru Kanagawa, Tamiko Matsui, Shiro Yoshida, and Eugene Malveaux for their assistance in animal treatments; Akira Nakatani for discussing in the dosimetry study; Zhaobin Zhang for providing the cell cultures; and Sachiko Naito and Veron M. Camp for their assistance.

REFERENCES

1. Jemal A, Siegel R, Ward E, et al. Cancer statistics, 2006. *CA Cancer J Clin.* 2006;56:106–130.
2. Chang CH, Wu HC, Tsai JJ, Shen YY, Changlai SP, Kao A. Detecting metastatic pelvic lymph nodes by ^{18}F-2-deoxyglucose positron emission tomography in patients with prostate-specific antigen relapse after treatment for localized prostate cancer. *Urol Int.* 2003;70:311–315.
3. Heicappell R, Muller-Mattheis V, Reinhardt M, et al. Staging of pelvic lymph nodes in neoplasms of the bladder and prostate by positron emission tomography with 2-[^{18}F]-2-deoxy-D-glucose. *Eur Urol.* 1999;36:582–587.
4. Hoh CK, Seltzer MA, Franklin J, deKernion JB, Phelps ME, Belldegrun A. Positron emission tomography in urological oncology. *J Urol.* 1998;159:347–356.
5. Oyama N, Akino H, Suzuki Y, et al. The increased accumulation of [^{18}F]fluorodeoxyglucose in untreated prostate cancer. *Jpn J Clin Oncol.* 1999; 29:623–629.
6. Hara T, Kosaka N, Kishi H. PET imaging of prostate cancer using carbon-11-choline. *J Nucl Med.* 1998;39:990–995.
7. Kato T, Tsukamoto E, Kuge Y, et al. Accumulation of [^{11}C]acetate in normal prostate and benign prostatic hyperplasia: comparison with prostate cancer. *Eur J Nucl Med Mol Imaging.* 2002;29:1492–1495.
8. Washburn LC, Sun TT, Anon JB, Hayes RL. Effect of structure on tumor specificity of alicyclic alpha-amino acids. *Cancer Res.* 1978;38:2271–2273.
9. Hubner KF, Krauss S, Washburn LC, Gibbs WD, Holloway EC. Tumor detection with 1-aminocyclopentane and 1-aminocyclobutane C-11-carboxylic acid using positron emission computerized tomography. *Clin Nucl Med.* 1981;6:249–252.
10. Washburn LC, Sun TT, Byrd B, Hayes RL, Butler TA. 1-Aminocyclobutane [^{11}C]carboxylic acid, a potential tumor-seeking agent. *J Nucl Med.* 1979;20: 1055–1061.
11. Shoup TM, Olson J, Hoffman JM, et al. Synthesis and evaluation of [^{18}F]1-amino-3-fluorocyclobutane-1-carboxylic acid to image brain tumors. *J Nucl Med.* 1999;40:331–338.

12. Schuster DM, Votaw JR, Nieh PT, et al. Initial experience with the radiotracer anti-1-amino-3-^{18}F-fluororacyclobutane-1-carboxylic acid with PET/CT in prostate carcinoma. *J Nucl Med.* 2007;48:56–63.
13. McConathy J, Voll RJ, Yu W, et al. Improved synthesis of *anti*-[^{18}F]FACBC: improved preparation of labeling precursor and automated radiosynthesis. *Appl Radiat Isot.* 2003;58:657–666.
14. Hamacher K, Coenen HH, Stocklin G. Efficient stereospecific synthesis of no-carrier-added 2-[^{18}F]-fluoro-2-deoxy-D-glucose using aminopolyether supported nucleophilic substitution. *J Nucl Med.* 1986;27:235–238.
15. Hrupka BJ, Lin YM, Gietzen DW, et al. Small changes in essential amino acid concentrations alter diet selection in amino acid-deficient rats. *J Nutr.* 1997;127:777–784.
16. Rau FC, Weber WA, Wester HJ, et al. O-(2-[^{18}F]fluoroethyl)- L-tyrosine (FET): a tracer for differentiation of tumour from inflammation in murine lymph nodes. *Eur J Nucl Med Mol Imaging.* 2002;29:1039–1046.
17. Blau M. Radiation dosimetry of 131-I-19-iodocholesterol: the pitfalls of using tissue concentration data [letter]. *J Nucl Med.* 1975;16:247–249.
18. Martarello L, McConathy J, Camp VM, et al. Synthesis of *syn*- and *anti*-1-amino-3-[^{18}F]fluoromethyl-cyclobutane-1-carboxylic acid (FMACBC), potential PET ligands for tumor detection. *J Med Chem.* 2002;45:2250–2259.
19. Verrey F. System L: heteromeric exchangers of large, neutral amino acids involved in directional transport. *Pflugers Arch.* 2003;445:529–533.
20. Schuster DM, Votaw JR, Nieh PT, et al. Initial experience with the radiotracer anti-1-amino-3-[^{18}F]fluorocyclobutane-1-carboxylic acid (anti-[^{18}F]FACBC) with PET/CT in newly diagnosed prostate cancer [abstract]. *J Nucl Med.* 2006(suppl); 47:224P.
21. Romeo E, Dave MH, Bacic D, et al. Luminal kidney and intestine SLC6 amino acid transporters of B^0AT-cluster and their tissue distribution in Mus musculus. *Am J Physiol Renal Physiol.* 2006;290:376–383.
22. Chillaron J, Estevez R, Mora C, et al. Obligatory amino acid exchange via systems bo,$^+$-like and y^+L-like: a tertiary active transport mechanism for renal reabsorption of cystine and dibasic amino acids. *J Biol Chem.* 1996;271:17761–17770.
23. Park SY, Kim JK, Kim IJ, et al. Reabsorption of neutral amino acids mediated by amino acid transporter LAT2 and TAT1 in the basolateral membrane of proximal tubule. *Arch Pharm Res.* 2005;28:421–432.
24. Bodoy S, Martin L, Zorzano A, Palacin M, Estevez R, Bertran J. Identification of LAT4, a novel amino acid transporter with system L activity. *J Biol Chem.* 2005;280:12002–12011.
25. Brenot-Rossi I, Bastide C, Garcia S, et al. Limited pelvic lymphadenectomy using the sentinel lymph node procedure in patients with localised prostate carcinoma: a pilot study. *Eur J Nucl Med Mol Imaging.* 2005;32:635–640.

JNM The Journal of NUCLEAR MEDICINE

A Preliminary Study of Anti-1-Amino-3-^{18}F-Fluorocyclobutyl-1-Carboxylic Acid for the Detection of Prostate Cancer

Shuntaro Oka, Ryota Hattori, Fumie Kurosaki, Masahito Toyama, Larry A. Williams, Weiping Yu, John R. Votaw, Yasunori Yoshida, Mark M. Goodman and Osamu Ito

J Nucl Med. 2007;48:46-55.

The Journal of Nuclear Medicine is published monthly.
SNMMI | Society of Nuclear Medicine and Molecular Imaging
1850 Samuel Morse Drive, Reston, VA 20190.
(Print ISSN: 0161-5505, Online ISSN: 2159-662X)

SNMMI SOCIETY OF NUCLEAR MEDICINE AND MOLECULAR IMAGING